ISSN 0915-633X

NATIONAL INSTITUTE FOR FUSION SCIENCE

Theoretical Study of Cylindrical Energy Analyzers for MeV Range Heavy Ion Beam Probes

A. Fujisawa and Y. Hamada

(Received – June 15, 1993)

NIFS-236 July 1993

RESEARCH REPORT
NIFS Series

This report was prepared as a preprint of work performed as a collaboration research of the National Institute for Fusion Science (NIFS) of Japan. This document is intended for information only and for future publication in a journal after some rearrangements of its contents.

Inquiries about copyright and reproduction should be addressed to the Research Information Center, National Institute for Fusion Science, Nagoya 464-01, Japan.

NAGOYA, JAPAN

Theoretical Study of Cylindrical Energy Analyzers for MeV Range Heavy Ion Beam Probes

A. Fujisawa and Y. Hamada

National Institute for Fusion Science

464-01, Furo-cho, Chikusa-ku, Nagoya, Japan

Abstract

A cylindrical energy analyzer with drift spaces is shown to have a second order focusing for beam incident angle when the deflection angle is properly chosen. The analyzer has a possibility to be applied to MeV range heavy ion beam probes, and will be also available for accurate particle energy measurements in many other fields.

Keywords: cylindrical energy analyzer, drift spaces, fringing field effects, second order focusing, resolution power, HIBP, 210° cylindrical analyzer

I. Introduction

The 30° parallel plate analyzers of the Proca and Green type[1,2], which posses a desirable feature of second order focus for beam incident angle, have been traditionally used for potential measurement of magnetically confined plasma with heavy ion beam probes (HIBP)[3–6]. The advancement of plasma confinement devices in size and magnetic field strength has compelled the probing beam energy to reach the MeV region[7]. It follows that the operation voltage has been approaching the practical limit of the Proca and Green type analyzer.

The cylindrical energy analyzer, whose focusing property is of first order, has a favorable characteristic that the operation voltage could be smaller than that of the 30° parallel plate analyzers. A prototype whose design was based on the widely known 127.3° cylindrical analyzer was built to investigate its applicability to the energy analyzer for HIBPs[8),9]. In these experiments the first order focusing was achieved and had a good agreement with a simulation result.

If drift spaces are added to both ends of the cylindrical deflector, as in the Proca and Green type analyzer, the focusing property may be improved to more than first order. The focusing property should be so excellent as to allow the spread in incident angles of the probing beams to observe different points in the target plasma. However, an essential difference between the cylindrical and the Proca and Green analyzers exists; in the cylindrical one the analyzed particles enter into the cylinder electrodes where the fringing field effects are significant. In this article, we will pursue a possibility to improve the focusing property of cylindrical energy analyzers with drift spaces, and will describe the

importance of the fringing field at the ends of the cylinder.

II. Mathematical Basis of Charged Particle Motion in Cylindrical Deflector

i) First Order Equation

The equation describing a precise beam trajectory in a centrifugal electric field ($E_r(R) \propto 1/R$) is

$$\frac{\mathrm{d}^2R}{\mathrm{d}x^2} - \frac{2}{R}\left(\frac{\mathrm{d}R}{\mathrm{d}x}\right)^2 - \frac{R}{R_0^2} + \frac{R^3}{R_0^4}\left(\frac{M_0}{M}\right)^2 = 0 \,, \tag{1}$$

where R_0, $x(= R_0\phi)$, ϕ are the curvature of the mean trajectory, the path length, and the azimuthal coordinate, respectively, and $M_0 = R(0)V_{\|}(0)$ corresponds to the angular momentum. The derivation is described in the appendix.

By substituting $R(x) = R_0 + R_0\delta r_1(\phi) + R_0\delta r_2(\phi)$ $(\delta r_2(\phi) \ll \delta r_1(\phi) \ll 1)$ and $V_{\|}(\phi) = V_0 + V_0\delta v$ into the above equation, the first and second order equations of $\delta r_1(\phi)$, $\delta r_2(\phi)$ are

$$\delta r_1''(\phi) + 2\delta r_1(\phi) - 2\delta m_1(0) = 0 \,, \tag{2}$$

$$\delta r_2''(\phi) + 2\delta r_2(\phi) + K(\phi) = 0 \,, \tag{3}$$

where $r''(\phi)$ represents the second order derivative, and

$$K(\phi) = 3\delta r_1^2(\phi) - 2\delta r_1'^2(\phi) - 6\delta m_1(0)\delta r_1 + 3\delta m_1(0)^2 - 2\delta m_2(0) \,, \tag{4}$$

$$\delta m_1(0) = \Delta r(0) + \Delta v(0) \,, \tag{5}$$

$$\delta m_2(0) = \Delta r(0)\Delta v(0) \,. \tag{6}$$

The first order solution of Eq. (1) is easily obtained as

$$\delta r_1(\phi) = \Delta r(0) + \frac{\sin\sqrt{2}\phi}{\sqrt{2}}\Delta r'(0) + (1 - \cos\sqrt{2}\phi)\Delta v(0) \,, \tag{7}$$

$$\delta r_1'(\phi) = \cos\sqrt{2}\phi\Delta r'(0) + \sqrt{2}\sin\sqrt{2}\phi\Delta v(0) \,, \tag{8}$$

where $\Delta r(0)$, $\Delta r'(0)$, $\Delta v(0)$ represent the initial radial displacement, the initial slope of the beam $\mathrm{d}r/\mathrm{d}x(0)$ and the initial parallel velocity along the standard trajectory, respectively.

ii) Second Order Equation

The second order equation described by Eq. (3) is solved by finding the particular solution. The insertion of the first order solutions expressed by Eqs (7), (8) into Eq. (4) yields

$$K(\phi) = \left(-\frac{7}{4}\Delta r'^2 + \frac{7}{2}\Delta v^2\right)\cos 2\sqrt{2}\phi - \frac{7\sqrt{2}}{2}\Delta r'\Delta v \sin 2\sqrt{2}\phi - \frac{\Delta v^2}{2} - \frac{\Delta r'^2}{4} - 2\Delta r\Delta v \ . \tag{9}$$

Therefore, the particular solution of Eq. (3) is a linear combination of $\sin 2\sqrt{2}\phi$ and $\cos 2\sqrt{2}\phi$, and it is obtained as

$$\delta r_2^p(\phi) = \left(-\frac{7}{24}\Delta r'^2 + \frac{7}{12}\Delta v^2\right)\cos 2\sqrt{2}\phi - \frac{7\sqrt{2}}{12}\Delta r'\Delta v \sin 2\sqrt{2}\phi + \frac{\Delta v^2}{4} + \frac{\Delta r'^2}{8} + \Delta r\Delta v \ . \tag{10}$$

With the initial conditions of $\delta r_2(0) = 0$, $\delta r_2'(0) = 0$, the solution of Eq. (1) to second order is explicitly written as

$$\delta r(\phi) = \delta r_1(\phi) + \delta r_2(\phi) = \Delta r + \frac{\sin\sqrt{2}\phi}{\sqrt{2}}\Delta r' + (1-\cos\sqrt{2}\phi)\Delta v + \frac{1}{12}(7\cos\sqrt{2}\phi + 5)(1-\cos\sqrt{2}\phi)\Delta r'^2 - \frac{1}{6}(7\cos\sqrt{2}\phi + 2)(1-\cos\sqrt{2}\phi)\Delta v^2 + \frac{7\sqrt{2}}{6}\sin\sqrt{2}\phi(1-\cos\sqrt{2}\phi)\Delta r'\Delta v + (1-\cos\sqrt{2}\phi)\Delta r\Delta v \ . \tag{11}$$

Differentiating the above solution, we obtain

$$\delta r'(\phi) = \delta r'_1(\phi) + \delta r'_2(\phi) = \cos\sqrt{2}\phi\Delta r' + \sqrt{2}\sin\sqrt{2}\phi\Delta v$$
$$+ \frac{\sqrt{2}}{6}\sin\sqrt{2}\phi(7\cos\sqrt{2}\phi - 1)\Delta r'^2 - \frac{\sqrt{2}}{6}\sin\sqrt{2}\phi(14\cos\sqrt{2}\phi - 5)\Delta v^2$$
$$+ \frac{7}{3}(2\cos\sqrt{2}\phi + 1)(1 - \cos\sqrt{2}\phi)\Delta r'\Delta v + \sqrt{2}\sin\sqrt{2}\phi\Delta r\Delta v \ . \tag{12}$$

According to the conservation law of angular momentum, the difference between the parallel velocities before and after the cylindrical deflector is given by

$$\delta v(\phi) = \left(\frac{1+\delta m}{1+\delta r}\right) - 1$$
$$= (1 + \Delta r + \Delta v + \Delta r\Delta v)(1 - \delta r(\phi) + \delta r^2(\phi) + \cdots) - 1$$
$$= -\frac{\sin\sqrt{2}\phi}{\sqrt{2}}\Delta r' + \cos\sqrt{2}\phi\Delta v + \frac{1}{12}(1 - \cos\sqrt{2}\phi)^2\Delta r'^2$$
$$+ \frac{1}{3}(3\cos\sqrt{2}\phi + 1)(1 - \cos\sqrt{2}\phi)\Delta v^2 + \frac{\sin\sqrt{2}\phi}{\sqrt{2}}\Delta r\Delta r'$$
$$- \frac{\sqrt{2}}{6}\sin\sqrt{2}\phi(4 - \cos\sqrt{2}\phi)\Delta r'\Delta v \ . \tag{13}$$

The above expression gives all the information necessary to examine the focusing property to second order.

iii) 127.3° Cylindrical Energy Analyzer

When $x/R_0 = \phi_0 = \pi/\sqrt{2} = 127.3°$, Eq. (11) gives the radial displacement as follows,

$$\Delta r_{\text{exit}} = \delta r(127.3°) = \Delta r + 2\Delta v - \frac{1}{3}\Delta r'^2 + \frac{5}{3}\Delta v^2 + 2\Delta r\Delta v + \cdots \ . \tag{14}$$

The substitution of the conditions of $\Delta r = 0$, $\Delta r' \simeq \delta\theta$, $\Delta v \simeq -\delta\theta^2/2$, into

Eq. (14) yields

$$\Delta r_{\rm exit}(\delta\theta) = -\frac{4}{3}\delta\theta^2 + \cdots \ . \tag{15}$$

The displacement is independent of the beam incident angle $\delta\theta$ to first order. Suppose that $\Delta r = \Delta r' = 0$, $\Delta v = \delta v \neq 0$, the velocity dependence is obtained as

$$\Delta r_{\rm exit}(\delta v) = 2.0\delta v + \frac{5}{3}\delta v^2 + \cdots \ . \tag{16}$$

Hence, the velocity resolution is known to be 2.

III. Fringing Field Effects

i) Model of Fringing Field

Beam particles entering into the drift space with a finite incident angle will obtain a potential energy at the entrance end of the cylinder, then the beam velocity will change by the potential according to the radial displacement. The velocity change will have a significant effect on the trajectories. Thus, an appropriate model of the fringing field is necessary to investigate the focusing property and the resolution power of the cylindrical energy analyzers.

In the vicinity of the cylinder entrance along the standard beam trajectory identical with $R = R_0$, the potential is expanded in Taylor series

$$\phi(x,\ y) = Ax + By + Cx^2 + Dxy + Ey^2 + \cdots \ , \tag{17}$$

where x, y are associated with r, $r\phi$, respectively. If the entrance plane is assumed to coincide with $y = 0$, the following restraints are imposed on the fringing field,

(1) On the entrance boundary, $\phi(x,\ 0) = -\phi(-x,\ 0)$, $E_x(x,\ 0) = -E_0$, $E_y(x,\ 0) = 0$.

(2) Fringing field is confined within the region of $-\delta < y < 0$, and on the boundary $E_x(x, -\delta) = 0$.

(3) On the standard trajectory identical with $x = 0$, the electric field points to the radial direction, that is, $E_y(0,\ y) = 0$.

(4) In the vicinity under consideration, the effect of the cylinder curvature is neglected, thus, the potential satisfies the Laplace's equation in the Euclid coordinate,

$$\Delta\phi = \frac{\partial^2\phi}{\partial x^2} + \frac{\partial^2\phi}{\partial y^2} = 0\ . \tag{18}$$

The fringing electric field satisfying these restraints is given by

$$\begin{aligned} &\phi_{\rm ent}(x,\ y) = E_0 x + \frac{E_0}{\delta} xy\ , \\ &E_x^{\rm ent}(x,\ y) = -E_0 - \frac{E_0}{\delta} y\ , \qquad (-\delta < y < 0) \\ &E_y^{\rm ent}(x,\ y) = -\frac{E_0}{\delta} x\ . \end{aligned} \tag{19}$$

ii) Charged Particle Motion in Fringing Field

The equation of the charged particle motion in the above electric field is described as

$$\begin{cases} m\dfrac{{\rm d}^2x}{{\rm d}t^2} = -q\dfrac{\partial\phi}{\partial x} = -qE_0 - q\dfrac{E_0}{\delta} y\ , \\ m\dfrac{{\rm d}^2y}{{\rm d}t^2} = -\dfrac{qE_0}{\delta} x\ . \end{cases} \tag{20}$$

By introducing new variables $\xi = x + y$, $\eta = x - y$, the equations are transformed into

$$\begin{cases} \ddot{\xi} = -\alpha - \beta^2\xi\ , \\ \ddot{\eta} = -\alpha + \beta^2\eta\ , \end{cases} \tag{21}$$

where $\alpha = qE_0/m$, $\beta = \sqrt{qE_0/m\delta}$, and $\ddot{\xi}$, $\ddot{\eta}$ mean the second order derivatives with respect to t.

For the charged particle with the initial conditions of $x_{\rm ent}(0) = \varepsilon$, $\dot{x}_{\rm ent}(0) = v_x$, $y_{\rm ent}(0) = -\delta$, $\dot{y}_{\rm ent}(0) = v_y$, the motion in the field is expressed as

$$x_{\rm ent}(t) = \varepsilon\Phi_c^+(\beta t) + \frac{v_x}{\beta}\Phi_s^+(\beta t) - \frac{v_y}{\beta}\Phi_s^-(\beta t)\ , \tag{22}$$

$$y_{\rm ent}(t) = -\varepsilon\Phi_c^-(\beta t) - \frac{v_x}{\beta}\Phi_s^-(\beta t) + \frac{v_y}{\beta}\Phi_s^+(\beta t) - \delta\ , \tag{23}$$

$$\dot{x}_{\rm ent}(t) = \varepsilon\beta\Phi_s^-(\beta t) + v_x\Phi_c^+(\beta t) - v_y\Phi_c^-(\beta t)\ , \tag{24}$$

$$\dot{y}_{\rm ent}(t) = -\varepsilon\beta\Phi_s^+(\beta t) - v_x\Phi_c^-(\beta t) + v_y\Phi_c^+(\beta t)\ , \tag{25}$$

where

$$\Phi_s^{\pm}(x) = \left(\frac{\sinh x \pm \sin x}{2}\right)\ ,\quad \Phi_c^{\pm}(x) = \left(\frac{\cosh x \pm \cos x}{2}\right)\ . \tag{26}$$

Similarly, if the fringing field at the exit of the cylinder is assumed to be

$$\begin{aligned}
&\phi_{\rm exit}(x,\ y) = E_0 x - \frac{E_0}{\delta}xy\ ,\\
&E_x^{\rm exit}(x,\ y) = -E_0 + \frac{E_0}{\delta}y\ ,\quad (0 < y < \delta)\\
&E_y^{\rm exit}(x,\ y) = \frac{E_0}{\delta}x\ .
\end{aligned} \tag{27}$$

the beam motion is described as

$$x_{\rm exit}(t) = \varepsilon\Phi_c^+(\beta t) - \delta\Phi_c^-(\beta t) + \frac{v_x}{\beta}\Phi_s^+(\beta t) + \frac{v_y}{\beta}\Phi_s^-(\beta t)\ , \tag{28}$$

$$y_{\rm exit}(t) = \varepsilon\Phi_c^-(\beta t) - \delta\Phi_c^+(\beta t) + \frac{v_x}{\beta}\Phi_s^-(\beta t) + \frac{v_y}{\beta}\Phi_s^+(\beta t) + \delta\ , \tag{29}$$

$$\dot{x}_{\rm exit}(t) = \varepsilon\beta\Phi_s^-(\beta t) - \delta\beta\Phi_s^+(\beta t) + v_x\Phi_c^+(\beta t) + v_y\Phi_c^-(\beta t)\ , \tag{30}$$

$$y_{\rm exit}(t) = \varepsilon\beta\Phi_s^+(\beta t) - \delta\beta\Phi_s^-(\beta t) + v_x\Phi_c^-(\beta t) + v_y\Phi_c^+(\beta t)\ , \tag{31}$$

with the initial conditions of $x_{\rm exit}(0) = \varepsilon$, $\dot{x}_{\rm exit}(0) = v_x$, $y_{\rm exit}(0) = 0$, $\dot{y}_{\rm exit}(0) = v_y$.

iii) Changes of Beam Parameters due to Fringing Field

The changes of beam parameters are estimated as

$$\Delta r_{\rm ent} = x(\delta/v), \quad \Delta r'_{\rm ent} = \frac{\dot{x}(\delta/v)}{\dot{y}(\delta/v)}, \quad \Delta v_{\rm ent} = y(\delta/v) - v_0 \ , \tag{32}$$

where $\Delta r_{\rm ent}$, $\Delta r'_{\rm ent}$, $\Delta v_{\rm ent}$ are the radial displacement from the standard trajectory, the slope $\mathrm{d}r/\mathrm{d}x$, and the parallel velocity just after the fringing field in the entrance side of the cylinder, respectively. Replacing ε, v_x, v_y with Δr, $\Delta v_\perp$, $v_0 + \Delta v$, these relations are reduced into

$$\Delta r_{\rm ent} = \Delta r + \delta \Delta r' \ , \tag{33}$$

$$\Delta r'_{\rm ent} = -\frac{\delta}{3}\Delta r + \Delta r' + \delta \Delta v - \frac{\delta}{2} \ , \tag{34}$$

$$\Delta v'_{\rm ent} = -\Delta r - \frac{\delta}{2}\Delta r' + \Delta v \ , \tag{35}$$

where we neglect higher terms than the first order of δ by assuming $\delta \ll 1$, and we use the following formula;

$$\begin{aligned} &\Phi_s^+(\beta t) \simeq \beta t + \cdots, \quad \Phi_s^-(\beta t) \simeq \frac{(\beta t)^3}{6} + \cdots, \\ &\Phi_c^+(\beta t) \simeq 1 + \cdots, \quad \Phi_c^-(\beta t) \simeq \frac{(\beta t)^2}{2} \cdots \ . \end{aligned} \tag{36}$$

Similarly, the changes of the beam parameters in the exit side of the cylinder due to the fringing field are given by

$$\Delta r_{\rm exit} = \Delta r + \delta \Delta r' \ , \tag{37}$$

$$\Delta r'_{\rm exit} = \frac{2\delta}{3}\Delta r + \Delta r' + \delta \Delta v - \frac{\delta}{2} \ , \tag{38}$$

$$\Delta v'_{\rm exit} = \Delta r + \frac{\delta}{2}\Delta r' + \Delta v \ , \tag{39}$$

where $\Delta r_{\rm exit}$, $\Delta r'_{\rm exit}$, $\Delta v_{\rm exit}$ are the radial displacement from the standard trajectory, the slope and the parallel velocity just after the fringing field in the exit side of the cylinder, respectively.

IV. Analysis of Focusing Property

i) Focusing Property without Fringing Field

In order to demonstrate the importance of the fringing field effects, first we neglect its effects completely. The boundary conditions at the entrance side of the cylinder are

$$\Delta r = h\tan\delta\theta \simeq h\delta\theta\ ,\quad \Delta r' = \tan\delta\theta \simeq \delta\theta\ ,\quad \Delta v = \cos\delta\theta - 1 \simeq -\frac{\delta\theta^2}{2}, \tag{40}$$

where h is the length of the drift space in the entrance side of the cylinder. By substituting these relations into Eqs. (11), (12), the radial displacement and the slope on the exit boundary of the cylinder are

$$\delta r(\phi_0) = \left(h + \frac{\sin\sqrt{2}\phi_0}{\sqrt{2}}\right)\delta\theta + \left(\frac{1-\cos\sqrt{2}\phi_0}{12}\right)(7\cos\sqrt{2}\phi_0 - 1)\delta\theta^2\ , \tag{41}$$

$$\delta r'(\phi_0) = \cos\sqrt{2}\phi_0\delta\theta + \frac{\sqrt{2}}{6}\sin\sqrt{2}\phi_0(7\cos\sqrt{2}\phi_0 - 4)\delta\theta^2\ , \tag{42}$$

where ϕ_0 is the angle length of the cylindrical deflector. The radial displacement on the exit plane of the analyzer is

$$\Delta r_{\rm exit}(\phi_0,\ \delta\theta) = \delta r(\phi_0) + l\delta r'(\phi_0) = \left(h + \frac{\sin\sqrt{2}\phi_0}{\sqrt{2}} + l\cos\sqrt{2}\phi_0\right)\delta\theta$$
$$+ \left[\frac{\sqrt{2}}{6}l\sin\sqrt{2}\phi_0(\cos\sqrt{2}\phi_0 - 4) + \frac{1}{12}(1-\cos\sqrt{2}\phi_0)(7\cos\sqrt{2}\phi_0 - 1)\right]\delta\theta^2\ , \tag{43}$$

where l is the length of the drift space in the exit side of the cylinder. The second order focusing is realized when

$$h(\phi_0) = -l\cos\sqrt{2}\phi_0 - \frac{\sin\sqrt{2}\phi_0}{\sqrt{2}}$$
$$= \frac{\sqrt{2}(1-\cos\sqrt{2}\phi_0)(7\cos^2\sqrt{2}\phi_0 + 7\cos\sqrt{2}\phi_0 - 8)}{4\sin\sqrt{2}\phi_0(7\cos\sqrt{2}\phi_0 - 4)}\ , \tag{44}$$

$$l(\phi_0) = \frac{\sqrt{2}}{4}\frac{(\cos\sqrt{2}\phi_0 - 1)(7\cos\sqrt{2}\phi_0 - 1)}{\sin\sqrt{2}\phi_0(7\cos\sqrt{2}\phi_0 - 4)}\ . \tag{45}$$

The solutions to satisfy $1 \geq h,\ l > 0$ exist in the two regions of ϕ_0;

$$\text{i) } 153.73^\circ \leq \phi_0 \leq 196.73^\circ, \quad \text{ii) } 221.22^\circ \leq \phi_0 \leq 254.56^\circ.$$

By solving Eq. (1) numerically with the conditions of Eq. (40), the focusing property of higher than second order is obtained in a power series of $\delta\theta$

$$\begin{aligned} \Delta r_{\text{exit}}(\phi_0, \delta\theta) &= \delta r(\phi_0, \delta\theta) + l\ \delta r'(\phi_0, \delta\theta) \\ &= c_1(\phi_0)\delta\theta + c_2(\phi_0)\delta\theta^2 + c_3(\phi_0)\delta\theta^3 + \cdots , \end{aligned} \tag{46}$$

where $c_1(\phi_0) = c_2(\phi_0) = 0$ is met here since the second order focusing is fulfilled. Figures 2, 3 demonstrate the results in the regions of $150^\circ < \phi_0 < 200^\circ$, $220^\circ \leq \phi_0 \leq 260^\circ$, respectively; (a)the focal lengths $l(\phi_0)$, $h(\phi_0)$, (b) the third order coefficient $c_3(\phi_0)$ and the resolution power estimated by

$$\frac{\partial \Delta r_{\text{exit}}}{\partial v}(\phi_0) = 1 - \cos\sqrt{2}\phi_0 + \sqrt{2}l \sin\sqrt{2}\phi_0 \ . \tag{47}$$

For simplicity, the velocity resolution is denoted as $\mathrm{d}r/\mathrm{d}v$ in figures. The resolution power of the analyzers around $\phi_0 \simeq 170^\circ$ is about one ($\mathrm{d}r/\mathrm{d}v \simeq 1$), while that around $\phi_0 = 240^\circ$ is nearly zero. In the range from 150° to about 180°, the coefficient $c_3(\phi_0)$ decreases monotonically, and changes its sign at $\phi_0 = 169.40^\circ$. At this deflection angle, the corresponding cylindrical analyzer ($h = 0.80$, $l = 0.37$) seems to have a third order focusing for incident angle. However, this condition can not be realized, as we will show later, if the fringing field effect is taken into account.

ii) Focusing Property in the case of $\delta = 0$

If we assume that the size of the fringing field region can be neglected, Eqs. (33-35), (37-39) show that only the potential effect remains in the entrance and

exit boundaries of the cylinder. From Eqs. (33-35) with $\delta = 0$, the boundary conditions at the entrance of the cylinder are

$$\Delta r = h\tan\delta\theta \simeq h\delta\theta,\ \ \Delta r' = \tan\delta\theta \simeq \delta\theta,$$
$$\Delta v = -h\tan\delta\theta + (\cos\delta\theta - 1) \simeq -h\delta\theta - \frac{\delta\theta^2}{2}\,. \tag{48}$$

Substituting these conditions into Eqs. (11), (12) we have

$$\delta r(\phi_0) = \alpha_1(\phi_0)\delta\theta + \alpha_2(\phi_0)\delta\theta^2 + \cdots, \tag{49}$$

$$\delta r'(\phi_0) = \alpha_1'(\phi_0)\delta\theta + \alpha_2'(\phi_0)\delta\theta^2 + \cdots, \tag{50}$$

then the radial displacement on the exit plane of the analyzer is given by

$$\begin{aligned}\Delta r_{\rm exit}(\phi_0,\ \delta\theta) &= \delta r(\phi_0) + l\delta r'(\phi_0)\\ &= \alpha_1(\phi_0)\delta\theta + \alpha_2(\phi_0)\delta\theta^2 + l\left[\alpha_1'(\phi_0)\delta\theta + \alpha_2'(\phi_0)\delta\theta^2\right]\,,\end{aligned} \tag{51}$$

where

$$\alpha_1(\phi_0) = h\cos(\sqrt{2}\phi_0) + \frac{\sin\sqrt{2}\phi_0}{\sqrt{2}}\,, \tag{52}$$

$$\alpha_1'(\phi_0) = -\sqrt{2}h\sin\sqrt{2}\phi_0 + \cos\sqrt{2}\phi_0\,, \tag{53}$$

$$\begin{aligned}\alpha_2(\phi_0) = \left[\frac{1-\cos\sqrt{2}\phi_0}{12}\right]\Big[&-(14\cos\sqrt{2}\phi_0 + 16)h^2\\ &- 14\sqrt{2}\sin\sqrt{2}\phi_0 h + 7\cos\sqrt{2}\phi_0 - 1\Big]\,,\end{aligned} \tag{54}$$

$$\begin{aligned}\alpha_2'(\phi_0) = \frac{\sqrt{2}}{12}\Big[&-(14\sin 2\sqrt{2}\phi_0 + 2\sin\sqrt{2}\phi_0)h^2\\ &+14\sqrt{2}(\cos 2\sqrt{2}\phi_0 - \cos\sqrt{2}\phi_0)h + 7\sin 2\sqrt{2}\phi_0 - 8\sin\sqrt{2}\phi_0\Big]\,,\end{aligned} \tag{55}$$

The identical equation $\Delta r_{\rm exit}(\phi_0,\ \delta\theta) \equiv 0$ yields,

$$l = -\frac{\alpha_1(\phi_0)}{\alpha_1'(\phi_0)} = -\frac{\alpha_2(\phi_0)}{\alpha_2'(\phi_0)}\,. \tag{56}$$

The relation $l = -\alpha_1(\phi_0)/\alpha_1'(\phi_0)$ gives the first order focusing condition as

$$l = \frac{h\cos\sqrt{2}\phi_0 + (1/\sqrt{2})\sin\sqrt{2}\phi_0}{\sqrt{2}h\sin\sqrt{2}\phi_0 - \cos\sqrt{2}\phi_0}\,. \tag{57}$$

The second order focusing condition is achieved when the following equation is satisfied;

$$\begin{aligned}
12(\alpha_1'\alpha_2 - \alpha_1\alpha_2') &= 2\sqrt{2}\sin\sqrt{2}\phi_0(7\cos^2\sqrt{2}\phi_0 + 8)h^3 \\
&\quad - (14\cos^3\sqrt{2}\phi_0 - 28\sin\sqrt{2}\phi_0\cos^2\sqrt{2}\phi_0 + 16\cos\sqrt{2}\phi_0 - 30)h^2 \\
&\quad + \sqrt{2}\sin\sqrt{2}\phi_0(14\sin^2\sqrt{2}\phi_0 - 7\cos^2\sqrt{2}\phi_0 + 1)h \\
&\quad - 7\cos^3\sqrt{2}\phi_0 - 14\sin^2\sqrt{2}\phi_0\cos\sqrt{2}\phi_0 - \cos\sqrt{2}\phi_0 + 8 \\
&= \sin\sqrt{2}\phi_0\left[h - \frac{\cos\sqrt{2}\phi_0 - 1}{\sqrt{2}\sin\sqrt{2}\phi_0}\right]\left[\sqrt{2}(14\cos^2\sqrt{2}\phi_0 + 16)h^2\right. \\
&\left. +14\sin\sqrt{2}\phi_0(2\cos\sqrt{2}\phi_0 + 1)h - \sqrt{2}(7\cos^2\sqrt{2}\phi_0 + 7\cos\sqrt{2}\phi_0 - 8)\right] = 0 .
\end{aligned} \tag{58}$$

This equation is divided into two factors,

$$h - \frac{1}{\sqrt{2}}\left(\frac{\cos\sqrt{2}\phi_0 - 1}{\sin\sqrt{2}\phi_0}\right) = 0 , \tag{59}$$

$$\begin{aligned}
&\sqrt{2}(14\cos^2\sqrt{2}\phi_0 + 16)h^2 + 14\sin\sqrt{2}\phi_0(2\cos\sqrt{2}\phi_0 + 1)h \\
&\qquad -\sqrt{2}(7\cos^2\sqrt{2}\phi_0 + 7\cos\sqrt{2}\phi_0 - 8) = 0 .
\end{aligned} \tag{60}$$

The first equation has a positive solution when the deflection angle ϕ_0 is larger than 127.3°. The substitution of h in Eq. (59) into Eq. (57) yields the relation $l = h = (\cos\sqrt{2}\phi_0 - 1)/\sqrt{2}\sin\sqrt{2}\phi_0$, then the velocity resolution power is

$$\frac{\partial\Delta r_{\text{exit}}}{\partial v}(\phi_0,\ \delta v) = 1 - \cos\sqrt{2}\phi_0 + \sqrt{2}l\sin\sqrt{2}\phi_0 = 0 . \tag{61}$$

Thus, the solution is not available for an energy analyzer. On the other hand, the second quadratic equation has solutions in the range of $0 < \phi_0 < 45.70°$, $208.86° < \phi_0 < 300.25°$, and the solutions have an interesting feature; if h is a solution of Eq. (60), the counterpart l given by Eq. (57) is also the other solution of Eq. (60). The solutions of Eqs. (57), (60) are found to be positive in the region of $208.86° < \phi_0 < 221.23°$, thus, we need not to investigate

the solution in the angle range of $0 \leq \phi_0 \leq 45.70°$ further. Hence, the three branches of solutions of Eq. (58) are distinguished as follows; i) $h = l$, ii) $h > l$, iii) $h < l$.

Figure 4 shows the focal length in the branch of $h = l$, and the third order coefficient $c_3(\phi_0)$ defined in Eq. (46). Note that in this branch the third order focusing is realized at $\phi_0 = 200.43°$. Figure 5 shows the properties of the other branches in the region of $200° \leq \phi_0 \leq 230°$; (a)the focal lengths l and h, and (b)the third order coefficients $c_3(\phi_0)$ and (c) the resolution power $\mathrm{d}r/\mathrm{d}v(\phi_0)$ in both cases of $h > l$, $h < l$. The dashed lines in these figures mean the region where the focal length is negative. In the $h > l$ branch, the third order focusing condition $c_3(\phi_0) = 0$ is accomplished at $\phi_0 = 210.37°$ with the resolution power of 0.18, when $h = 0.60$, $l = 0.29$. On the other hand, the third order coefficient in the $h < l$ branch becomes zero at $\phi_0 = 222.60°$, however, the corresponding h is less than zero.

The analysis here containing the potential effect of the fringing field presents completely different properties from those with no fringing field effect. The potential effect plays a significant role on even the first order focusing property of the cylindrical analyzer.

iii) Focusing Property of Fringing Field with $\delta \neq 0$

If we take into account a small but finite size of the fringing field region,

the boundary conditions are

$$\Delta r = (h+\delta)\tan\delta\theta \simeq (h+\delta)\delta\theta \ ,$$
$$\Delta r' = -\frac{\delta}{2} + \left(1 - \frac{\delta\, h}{3}\right)\tan\delta\theta + \delta(\cos\delta\theta - 1) \simeq -\frac{\delta}{2} + \left(1 - \frac{\delta\, h}{3}\right)\delta\theta - \frac{\delta}{2}\delta\theta^2 \ ,$$
$$\Delta v = -\left(h + \frac{\delta}{2}\right)\tan\delta\theta + (\cos\delta\theta - 1) \simeq -\left(h + \frac{\delta}{2}\right)\delta\theta - \frac{\delta\theta^2}{2} \ . \tag{62}$$

The substitution of the conditions into Eqs.(11-13) gives the functions $\delta r(\phi_0)$, $\delta r'(\phi_0)$, $\delta v(\phi_0)$ in the following form;

$$\delta r(\phi_0) = \alpha_0(\phi_0) + \alpha_1(\phi_0)\delta\theta + \alpha_2(\phi_0)\delta\theta^2 + \cdots, \tag{63}$$

$$\delta r'(\phi_0) = \alpha_0'(\phi_0) + \alpha_1'(\phi_0)\delta\theta + \alpha_2'(\phi_0)\delta\theta^2 + \cdots, \tag{64}$$

$$\delta v(\phi_0) = \beta_0(\phi_0) + \beta_1(\phi_0)\delta\theta + \beta_2(\phi_0)\delta\theta^2 + \cdots. \tag{65}$$

By taking Eq. (37-39) into consideration, the radial displacement on the exit plane is described as

$$\begin{aligned}\Delta r_{\rm exit}(\phi_0,\ \delta\theta) &= \left(1 + \frac{2\delta\, l}{3}\right)\delta r(\phi_0) + (l+\delta)\delta r'(\phi_0) + \delta\ l\delta v(\phi_0) - \frac{\delta\, l}{2} \\ &= \Gamma_0(\phi_0) - \frac{\delta\, l}{2} + \Gamma_1(\phi_0)\delta\theta + \Gamma_2(\phi_0)\delta\theta^2 + \cdots \ ,\end{aligned} \tag{66}$$

where

$$\Gamma_i(\phi_0) = \alpha_i(\phi_0) + \delta\alpha_i'(\phi_0) + l\,[\alpha_i'(\phi_0) + \delta(\beta_i(\phi_0) + 2\alpha_i(\phi_0)/3)] \ . \tag{67}$$

Thus, the finite size of the fringing field region should give rise to the offset of the beam exit position which is given by

$$\begin{aligned}\Delta r_{\rm offset}(\phi_0,\ \delta) &= \Gamma_0(\phi_0) - \frac{\delta\, l}{2} \\ &= \alpha_0(\phi_0) + \delta\,\alpha_0'(\phi_0) + l\,[\alpha_0' + \delta\,(\beta_0 + (2/3)\alpha_0 - 1/2)] \ .\end{aligned} \tag{68}$$

From $\Delta r_{\rm exit} \equiv 0$, we have the second order focusing condition

$$l = -\frac{\alpha_1(\phi_0) + \delta\,\alpha_1'(\phi_0)}{\alpha_1' + \delta\,(\beta_1(\phi_0) + 2\alpha_1(\phi_0)/3)} = -\frac{\alpha_2(\phi_0) + \delta\,\alpha_2'(\phi_0)}{\alpha_2' + \delta\,(\beta_2(\phi_0) + 2\alpha_2(\phi_0)/3)}\,. \quad (69)$$

The explicit forms of the functions $\alpha(\phi_0)$, $\alpha'(\phi_0)$, $\beta(\phi_0)$, can not be obtained from the second order solution of Eqs. (11-13) since higher order terms $\Delta r'^3$, $\Delta r'^2\Delta v$, *etc.* contribute to these functions. To the extent of our approximation, the functions are described as

$$\alpha_0(\phi_0) = -\frac{\sqrt{2}\delta}{4}\sin\sqrt{2}\phi_0 + \frac{\delta^2}{48}(-7\cos^2\sqrt{2}\phi_0 + 2\cos\sqrt{2}\phi_0 + 5) + o(\delta^3) + \cdots\,, \quad (70)$$

$$\alpha_1(\phi_0) = h\left[\cos\sqrt{2}\phi_0 + \frac{\sqrt{2}\delta}{12}\sin\sqrt{2}\phi_0(5 - 7\cos\sqrt{2}\phi_0) + o(\delta^2) + \cdots\right] + \frac{\sin\sqrt{2}\phi_0}{\sqrt{2}} + \frac{\delta}{12}(7\cos^2\sqrt{2}\phi_0 + 4\cos\sqrt{2}\phi_0 + 1) + o(\delta^2) + \cdots\,, \quad (71)$$

$$\alpha_2(\phi_0) = h^2\left[\frac{1}{6}(7\cos\sqrt{2}\phi_0 + 8)(\cos\sqrt{2}\phi_0 - 1) + o(\delta) + \cdots\right] + h\left[\frac{7\sqrt{2}}{6}\sin\sqrt{2}\phi_0(\cos\sqrt{2}\phi_0 - 1) + o(\delta) + \cdots\right] + \frac{1}{12}(1 - \cos\sqrt{2}\phi_0)(7\cos\sqrt{2}\phi_0 - 1) + o(\delta) + \cdots\,, \quad (72)$$

$$\alpha_0'(\phi_0) = -\frac{\delta}{2}\cos\sqrt{2}\phi_0 + \frac{\sqrt{2}}{24}\delta^2\sin\sqrt{2}\phi_0(7\cos\sqrt{2}\phi_0 - 1) + o(\delta^3) + \cdots\,, \quad (73)$$

$$\alpha_1'(\phi_0) = h\left[-\sqrt{2}\sin\sqrt{2}\phi_0 - \frac{\delta}{6}(14\cos^2\sqrt{2}\phi_0 - 5\cos\sqrt{2}\phi_0 - 7) + o(\delta^2) + \cdots\right] + \cos\sqrt{2}\phi_0 - \frac{\sqrt{2}\delta}{6}\sin\sqrt{2}\phi_0(7\cos\sqrt{2}\phi_0 + 2) + o(\delta^2) + \cdots\,, \quad (74)$$

$$\alpha_2'(\phi_0) = h^2\left[-\frac{\sqrt{2}}{6}(7\sin 2\sqrt{2}\phi_0 + \sin\sqrt{2}\phi_0) + o(\delta) + \cdots\right] + h\left[\frac{7\sqrt{2}}{6}(\cos 2\sqrt{2}\phi_0 - \cos\sqrt{2}\phi_0) + o(\delta) + \cdots\right] + \frac{\sqrt{2}}{12}(7\sin 2\sqrt{2}\phi_0 - 8\sin\sqrt{2}\phi_0) + o(\delta) + \cdots\,, \quad (75)$$

$$\beta_0(\phi_0) = \frac{\sqrt{2}}{4}\delta \sin\sqrt{2}\phi_0 + \frac{\delta^2}{48}(1-\cos\sqrt{2}\phi_0)^2 + o(\delta^3) + \cdots , \tag{76}$$

$$\begin{aligned}\beta_1(\phi_0) = h&\left[-\cos\sqrt{2}\phi_0 + \frac{\sqrt{2}}{12}\delta\sin\sqrt{2}\phi_0(\cos\sqrt{2}\phi_0 - 5) + o(\delta^2) + \cdots\right] \\ &-\frac{1}{\sqrt{2}}\sin\sqrt{2}\phi_0 - \frac{\delta}{12}(\cos^2\sqrt{2}\phi_0 + 4\cos\sqrt{2}\phi_0 + 1) + o(\delta^2) + \cdots .\end{aligned} \tag{77}$$

$$\begin{aligned}\beta_2(\phi_0) = h^2&\left[\frac{1}{3}(1-\cos\sqrt{2}\phi_0)(3\cos\sqrt{2}\phi_0 + 1) + o(\delta) + \cdots\right] \\ &+ h\left[\frac{\sqrt{2}}{6}\sin\sqrt{2}\phi_0(7 - \cos\sqrt{2}\phi_0) + o(\delta) + \cdots\right] \\ &+ \frac{1}{12}(\cos^2\sqrt{2}\phi_0 - 8\cos\sqrt{2}\phi_0 + 1) + o(\delta) + \cdots ,\end{aligned} \tag{78}$$

Although the exact expression of Eq. (69), or the explicit second order focusing condition, can not be given, it is possible to find the focal lengths h, l at a given ϕ_0. By solving Eq. (1) numerically with the boundary conditions indicated by Eq. (62), the dependence of the radial displacement on the beam incident angle can be obtained at a given pair of h, l in a power series as expressed by Eq. (47). Several iterations at a fixed ϕ_0 yield the focal lengths h, l consistent with $c_1(\phi_0) = c_2(\phi_2) = 0$. The initial values of h, l are chosen to satisfy Eq. (59) since the solutions should exist in the vicinity of them when $\delta \ll 0$. After finding a pair of the lengths h, l to accomplish the second order focusing, the resolution power should be also numerically calculated by solving Eq. (1) with the boundary conditions of $\Delta r = 0$, $\Delta r' = -\delta/2$, $\Delta v = \delta v$. From Eqs. (37-39), the radial displacement on the exit plane is written in a similar form to Eq. (66), and is expanded in a power series of δv

$$\begin{aligned}\Delta r_{\rm exit}(\phi_0,\ \delta v) &= \left(1 + \frac{2\delta\, l}{3}\right)\delta r(\phi_0) + (l+\delta)\delta r'(\phi_0) + \delta\, l\delta v(\phi_0) - \frac{\delta\, l}{2} \\ &= c_{v0}(\phi_0) + c_{v1}(\phi_0)\delta v + c_{v2}(\phi_0)\delta v^2 + \cdots ,\end{aligned} \tag{79}$$

hence, the resolution power is $\mathrm{d}\Delta r_{\rm exit}/\mathrm{d}v = c_{v1}(\phi_0)$.

We will deal with the case of $\delta = 0.05$ first. Equation (69) has at least a real solution at a given ϕ_0, since it is a cubic equation of h. The solution is defined here as h_1, l_1. Figure 6 shows a positive pair of h_1, l_1 in the region of $180° < \phi_0 < 220°$, and the corresponding third order coefficient $c_3(\phi_0)$ and the resolution power $\mathrm{d}r/\mathrm{d}v$. In the deflection angle bellow $\phi_0 \simeq 205°$ the focal lengths h_1 and l_1 are associated with the $h = l$ branch of the previous case with $\delta = 0$, and in the region above this angle the solution seems to connect to the $h < l$ branch. The focal length h_1 is positive in $\phi_0 \leq 218.00°$, and the third order focusing $c_3(\phi_0) = 0$ is realized at $\phi_0 = 200.80°$, $218.79°$. Neither of the angles is, however favorable for an energy analyzer since the resolution power at $\phi_0 = 200.80°$ is nearly zero, similarly to the $h = l$ branch of $\delta = 0$, and the focal length h_1 at $\phi_0 = 218.79°$ is negative. Thus, in this branch, the analyzer with $\phi_0 \simeq 210°$ will be suitable owing to smaller third order coefficient $c_3(\phi_0)$ and larger velocity resolution $\mathrm{d}r/\mathrm{d}v$.

The other branches of solutions are found in the region larger than $\phi_0 \simeq 210°$. Figure 7 shows pairs of the focal lengths (h_2, l_2) and (h_3, l_3), and their third order coefficients and the resolution powers. The pairs of (h_2, l_2), (h_3, l_3) are associated with the $h = l$, $h > l$ branches of $\delta = 0$, respectively. The branch of h_2, l_2 is not desirable since the resolution power is nearly zero. In the other branch the focal lengths h_3, l_3 are positive when $\phi_0 \leq 218.03°$, and the third order focusing is achieved at $\phi_0 = 211.22°$ with the resolution power of 0.18.

As for the case of $\delta = 0.10$, there will be three branches of the solutions. The focal lengths of the h_1-branch are also indicated in Fig. 8, together with the third order coefficient $c_3(\phi_0)$ and the resolution power $\mathrm{d}r/\mathrm{d}v$. The dependences

of h_1, l_1, c_3, $\mathrm{d}r/\mathrm{d}v$ on the deflection angle ϕ_0 are very similar to the case of $\delta = 0.05$. The third order focusing is fulfilled at $\phi_0 = 201.04°$ (in the previous two cases, $\phi_0 = 200.43°$, $200.80°$ when $\delta = 0.0$, 0.05, respectively), and h_1 becomes zero at $\phi_0 = 215.47°$ ($\phi_0 = 221.23°$, $218.03°$ when $\delta = 0.0$, 0.05, respectively). The other branches of (h_2, l_2), (h_3, l_3), as shown in Fig. 9, also have the qualitatively similar tendency as the corresponding branches of $\delta = 0.05$. In the h_2-branch which corresponds to the $h = l$ branch of $\delta = 0$, the resolution power is so small for an energy analyzer. In the h_3-branch, the focal length h_3 is positive when $\phi_0 \leq 215.20°$ ($\phi_0 = 221.23°$, $218.00°$ when $\delta = 0.0$, 0.05, respectively), and the third order focusing is achieved at $\phi_0 = 211.17°$ with the resolution power of 0.17 ($\phi_0 = 210.37°$, $211.22°$, when $\delta = 0.0$, 0.05, respectively).

Finite sizes of the fringing field region alter the focal lengths and the resolution power, however, the basic dependence of the focusing property on the deflection angle is not changed. The most important effect of the fringing field, therefore, is the radially directed potential difference which changes the entering particle velocity according to the radial deviation from the standard trajectory on the entrance boundary of the cylinder.

V. Discussion

The analysis including the fringing field shows that the second order focusing for beam incident angle, even the third order focusing, can be realized at the proper deflection angle. However, the cylindrical analyzer with a deflection angle smaller than about 180°, which may be convenient to be designed and constructed, is of no use for an energy analyzer since their focal length rela-

tion $h \simeq l$ leads to nearly zero velocity resolution. We suppose here that the deflection angle $\phi_0 \simeq 210°$ should the minimum appropriate value providing a smaller third order coefficient a larger resolution power.

The characteristics of 210.0° cylindrical analyzers for three examples with the different fringing field region sizes of $\delta = 0$, $\delta = 0.05$, $\delta = 0.1$ are numerically calculated. In the case of $\delta = 0$, the second order focusing condition is realized when $h = 0.306$, $l = 0.585$, the focusing and resolution properties are

$$\Delta r_{\rm exit}(\delta\theta) = 0.20\delta\theta^3 - 0.41\delta\theta^4 + 0.76\delta\theta^5 + \cdots \tag{80}$$

$$\Delta r_{\rm exit}(\delta v) = -0.19\delta v - 0.31\delta v^2 + \cdots . \tag{81}$$

In the second case of $\delta = 0.05$, when the focal lengths $h = 0.217$, $l = 0.592$, the properties are

$$\Delta r_{\rm exit}(\delta\theta) = -0.0064 + 0.17\delta\theta^3 - 0.36\delta\theta^4 + 0.66\delta\theta^5 + \cdots, \tag{82}$$

$$\Delta r_{\rm exit}(\delta v) = -0.0064 - 0.28\delta v - 0.28\delta v^2 + \cdots , \tag{83}$$

In the third case of $\delta = 0.1$ when the focal lengths $h = 0.160$, $l = 0.552$, the properties are

$$\Delta r_{\rm exit}(\delta\theta) = -0.0113 + 0.15\delta\theta^3 - 0.36\delta\theta^4 + 0.66\delta\theta^5 + \cdots, \tag{84}$$

$$\Delta r_{\rm exit}(\delta v) = -0.0113 - 0.31\delta v - 0.27\delta v^2 + \cdots . \tag{85}$$

Figure 10 shows these focusing property for the beam incident angle and the velocity dependence of the exit position. Both focusing property and the resolution power become better with an increase of δ.

Sufficiently wide acceptance angle is an essential factor required for the energy analyzer of HIBPs since the incident angle of the probing beam into the analyzer varies with observation points unless the beam trajectories are controlled actively by some means[10]. If the beam enters into the analyzer

with a finite incident angle $\delta\theta$, the apparent energy shift ΔK is estimated by

$$\Delta K = K_0 \frac{2\delta V}{V_0} = 2K_0 \frac{\partial v}{\partial r}(\Delta r_{\rm exit}(\delta\theta) - \Delta r_{\rm offset}) \tag{86}$$

where K_0 is the initial beam energy. In the case of the 210° analyzer with $\delta = 0.1$, the insertion of $\partial r/\partial v = -0.31$, $(\Delta r_{\rm exit} - \Delta r_{\rm offset}) = 0.15\delta\theta^3$ into the above formula gives the expression of the apparent energy shift as $|\Delta K| = 0.97 K_0 \delta\theta^3$. If the potential is needed to be measured with precision of 10eV using 1MeV beam, the incident angle is accepted to be less than 1.2°. As for the 127.3° analyzer, the apparent energy shift is $|\Delta K| = 2 \times 0.5 \times 4/3 K_0 \delta\theta^2$ from Eqs. (15), (16), (86) then the maximum acceptance angle is 0.16° under the same condition. The 210° analyzer is more excellent to the 127.3° one in the acceptance angle property.

There remains a problem to examine the operation voltage of the cylindrical analyzers. The displacement of the beam with maximum acceptance angles restricts the gap width, that is,

$$\Delta R_{\rm gap} > 2\delta r_{\rm max}(\delta\theta_{\rm accept}) \ . \tag{87}$$

The voltages should satisfy

$$V_0 \simeq \frac{K_0}{q}\frac{\Delta R_{\rm gap}}{R_0} > \frac{2K_0}{q}\frac{\delta r_{\rm max}(\delta\theta_{\rm accept})}{R_0} \ , \tag{88}$$

where K_0, q, $\Delta R_{\rm gap}$ the beam energy in eV units, the charge of the beam, and the gap width between electrodes, respectively. When the beam has an incident angle of $\delta\theta_{\rm accept}$, Eqs. (49), (52) yields the description of the maximum displacement to first order as

$$\begin{aligned} \delta r_{\rm max}(\delta\theta_{\rm accept}) &= \max\left[R_0 \left(h\cos\sqrt{2}\phi + \frac{\sin\sqrt{2}\phi}{\sqrt{2}} \right) \delta\theta_{\rm accept} \right] \\ &= R_0 \sqrt{h^2 + \frac{1}{2}}\delta\theta_{\rm accept} \ , \end{aligned} \tag{89}$$

where $\delta = 0$ is assumed for simplicity. Equations (87-89) are combined into the following relation,

$$V_0 > V_{\min} = \frac{2K_0}{q} R_0 \sqrt{h^2 + \frac{1}{2}}\, \delta\theta_{\text{accept}} \ . \tag{90}$$

Hence, the operation voltage is reduced to a practical level if the acceptance angle is taken to be small. For the 210° cylindrical analyzer with $\delta = 0.0$, whose focal lengths are $h = 0.31$, $l = 0.59$, presumed that the acceptance of incident angle is $\pm 1.5°$ and the charge of beam $q = 2$, Eq. (90) gives $V_{\min} \simeq 0.020 K_0$. The voltage can be reduced to 1/40 of the beam energy, while the voltage of the 30° parallel plate analyzer is reduced to only 1/8.

The present analysis including a model of the fringing field shows that the cylindrical type analyzer should be applicable to MeV range HIBPs. A discrepancy between the model and the actual fringing fields, however, may alter the focusing condition. Thus, the geometry and structure at the ends of the cylinder should be most carefully designed to avoid unfavorable fringing electric fields and to make beam trajectories closer to the ones in the presented model. Before constructing a prototype, further analysis including numerically calculated fringing electric fields[8] with more accuracy is an indispensable work to realize the desired performance in the cylindrical energy analyzer equipped with two drift regions.

Acknowledgements

The authors would like to thank Dr. H. Iguchi and Dr. M. Sasao in National Institute for Fusion Science for their continuous encouragements.

Appendix

The Lagrangian in the cylindrical coordinate is

$$L = \frac{m}{2}(\dot{r}^2 + r^2\dot{\phi}^2) - q\psi \tag{A1}$$

where m, q, ψ are the mass, the charge of particle, the potential, respectively. The equations of motion are

$$\frac{\mathrm{d}}{\mathrm{d}t}\left(\frac{\partial L}{\partial \dot{r}}\right) - \frac{\partial L}{\partial r} = m\ddot{r} - mr\dot{\phi}_0^2 + q\frac{\partial \psi}{\partial r} = 0\,, \tag{A2}$$

$$\frac{\partial L}{\partial \dot{\phi}} = mr^2\dot{\phi} \equiv M = const.\,, \tag{A3}$$

where M is angular momentum. Substitution of $(A3)$ into $(A2)$ gives

$$m\ddot{r} - \frac{M^2}{mr^3} + \frac{qE_{r0}R_0}{r} = 0\,, \tag{A4}$$

where

$$E_r(r) = -\frac{\partial \psi}{\partial r} = \frac{E_{r0}R_0}{r}\,. \tag{A5}$$

In the reference beam whose trajectory is denoted as $r = R_0$, the angular momentum M_0 satisfies

$$\frac{M_0^2}{mR_0^3} = qE_{r0}\,. \tag{A6}$$

Changing the independent variable from t to $x = R_0\phi$ by the use of the relation

$$\frac{\mathrm{d}r}{\mathrm{d}t} = \frac{\mathrm{d}r}{\mathrm{d}\phi}\left(\frac{\mathrm{d}\phi}{\mathrm{d}t}\right) = \frac{M}{mr^2}\frac{\mathrm{d}r}{\mathrm{d}\phi}\,, \tag{A7}$$

we obtain the final expression

$$\frac{\mathrm{d}^2r}{\mathrm{d}x^2} - \frac{2}{r}\left(\frac{\mathrm{d}r}{\mathrm{d}x}\right)^2 - \frac{r}{R_0^2} + \frac{r^3}{R_0^4}\left(\frac{M_0}{M}\right)^2 = 0\,. \tag{A8}$$

References

1) T. S. Green and G. A. Proca, Rev. Sci. Instrum. 41, 1409(1970).

2) G. A. Proca and T. S. Green, Rev. Sci. Instrum. 41, 1778 (1970).

3) L. Solensten and K. A. Connor, Rev. Sci. Instrum. 58, 516(1987).

4) S. C. Aceto, K. A. Connor, P. E. McClaren, J. J. Zielinski, and J. G. Schatz, Rev. Sci. Instrum. 61, 2958(1990).

5) P. E. McClaren, K. A. Connor, J. F. Lewis, R. L. Hickok, T. P. Crowley, J. G. Schatz and G. H. Vilardi, Rev. Sci. Instrum. 61, 2955(1990).

6) Y. Hamada, Y. Kawasumi, K. Masai, H. Iguchi, A. Fujisawa, Y. Abe, Rev. Sci. Instrum. 63, 4446(1992).

7) P. M. Schoch, J. C. Forster, W. C. Jennings, and R. L. Hickok, Rev. Sci. Instrum. 57, 1825(1986).

8) K. A. Connor, T. P. Crowley, R. L. Hickok, A. Carnevali, P. M. Schoch, J. Resnick, V. Simcic, J. G. Schatz, J. Heard, S. C. Aceto and J. F. Lewis, Rev. Sci. Instrum. 59, 1673(1988).

9) H. J. Leisenfelder, R. L. Hickok, J. H. Resnick, T. P. Crowley, and J.G. Schatz, Rev. Sci. Instrum. 63, 4579(1992).

10) A. Fujisawa, H. Iguchi, M. Sasao, Y. Hamada and J. Fujita, Rev. Sci. Instrum. 63, 3694(1992).

Figure Captions

Fig. 1: Cylindrical energy analyzer equipped with drift space at both ends.

Fig. 2: Properties with no fringing field effects in the deflection angle of $150° < \phi_0 < 200°$. (a) Focal lengths $h(\phi_0)$, $l(\phi_0)$ to have a second order focusing, (b) the third order coefficient $c_3(\phi_0)$ in the power series of $\delta\theta$, and resolution power $\mathrm{d}r/\mathrm{d}v$.

Fig. 3: Properties with no fringing field effect in the deflection angle of $200° < \phi_0 < 260°$. (a) Focal lengths $l(\phi_0)$, $h(\phi_0)$ to have a second order focusing, (b)the third order coefficient $c_3(\phi_0)$, and the resolution power $\mathrm{d}r/\mathrm{d}v$

Fig. 4: Properties with the fringing field effect in the deflection angle of $170° \leq \phi_0 \leq 260°$. The size of the fringing field region is assumed to be zero. The open and close circles represent the focal lengths $h(\phi_0)$, $l(\phi_0)$ and the third order coefficient $c_3(\phi_0)$, respectively. The focal lengths of this case satisfy $h = l = (\cos\sqrt{2}\phi_0 - 1)/\sqrt{2}\sin\sqrt{2}\phi_0$, and this relation leads to zero velocity resolution.

Fig. 5: Properties with the fringing field effect in the deflection angle of $200° \leq \phi_0 \leq 230°$. The size of the fringing field region is assumed to be zero. (a) Focal lengths $h(\phi_0)$, $l(\phi_0)$ (b) third order coefficient $c_3(\phi_0)$ (c) velocity resolution $\mathrm{d}r/\mathrm{d}v(\phi_0)$. At a given ϕ_0, both combinations $h > l$, $h < l$ are possible to realized a second order focusing. The dashed lines mean the region where one of the focal lengths is negative.

Fig. 6: Properties with the fringing field effect in the deflection angle of $180° \leq \phi_0 \leq 220°$. the size of the fringing field region is assumed to be 0.05. (a) Focal lengths $h_1(\phi_0)$, $l_1(\phi_0)$ (b) the third order coefficient $c_3(\phi_0)$ and the resolution power $\mathrm{d}r/\mathrm{d}v(\phi_0)$. The dashed lines mean the region where one of the focal lengths is negative.

Fig. 7: Properties with the fringing field effect in the deflection angle of $210° \leq \phi_0 \leq 240°$. The size of the fringing field region is assumed to be 0.05. (a) Focal lengths $(h_2(\phi_0),\ l_2(\phi_0))$, $(h_3(\phi_0),\ l_3(\phi_0))$, (b) the third order coefficient $c_3(\phi_0)$ and the resolution power $\mathrm{d}r/\mathrm{d}v(\phi_0)$. The dashed lines mean the region where one of the focal lengths is negative.

Fig. 8: Properties with the fringing field effect in the deflection angle of $180° \leq \phi_0 \leq 220°$. The size of the fringing field region is assumed to be 0.1. (a) Focal lengths $h_1(\phi_0)$, $l_1(\phi_0)$ (b) the third order coefficient $c_3(\phi_0)$ and the resolution power $\mathrm{d}r/\mathrm{d}v(\phi_0)$. The dashed lines mean the region where one of the focal lengths is negative.

Fig. 9: Properties with the fringing field effect in the deflection angle of $210° \leq \phi_0 \leq 240°$. The size of the fringing field region is assumed to be 0.1. (a)Focal lengths $(h_2(\phi_0),\ l_2(\phi_0))$, $(h_3(\phi_0),\ l_3(\phi_0))$ (b) the third order coefficient $c_3(\phi_0)$ and the resolution power $\mathrm{d}r/\mathrm{d}v(\phi_0)$. The dashed lines mean the region where one of the focal lengths is negative.

Fig. 10: Characteristics of a cylindrical energy analyzer whose deflection angle is 210°; (a) dependence of exit position on incident angle, $\Delta r_{\mathrm{exit}}(\delta\theta)$ (b) resolution power $\Delta r_{\mathrm{exit}}(\delta v)$.

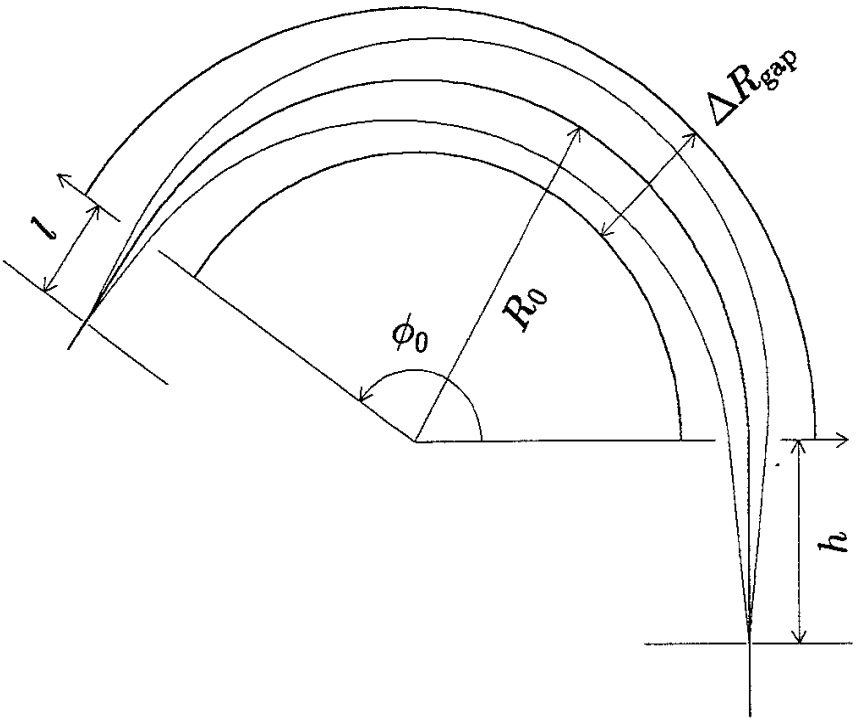

Fig. 1 A. Fujisawa and Y. Hamada

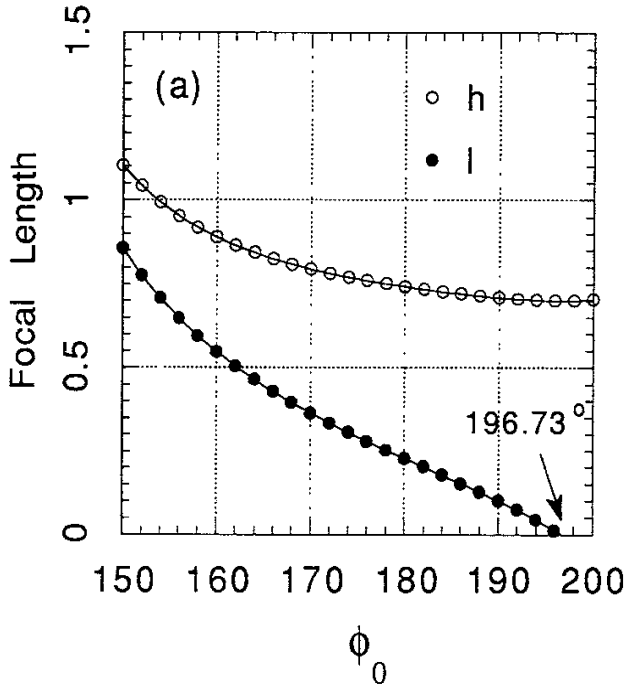

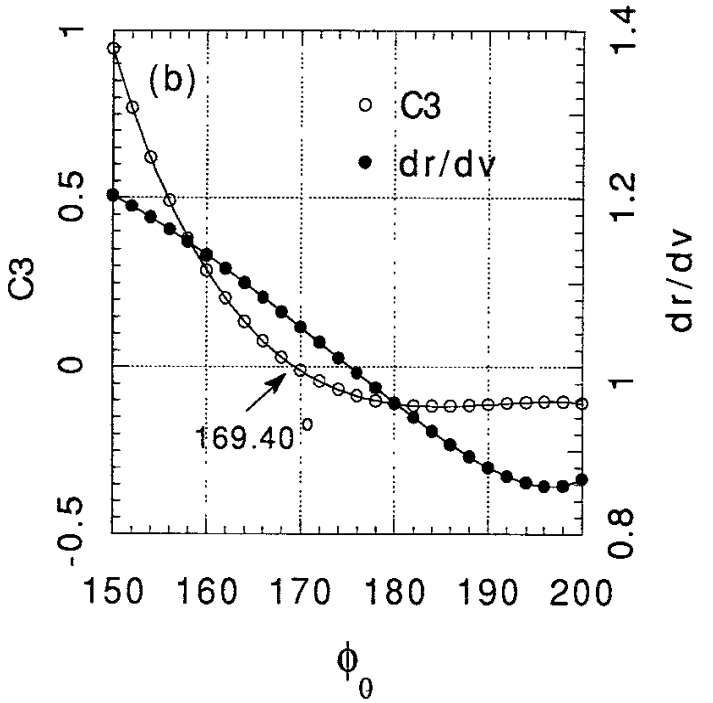

Fig. 2 A. Fujisawa and Y. Hamada

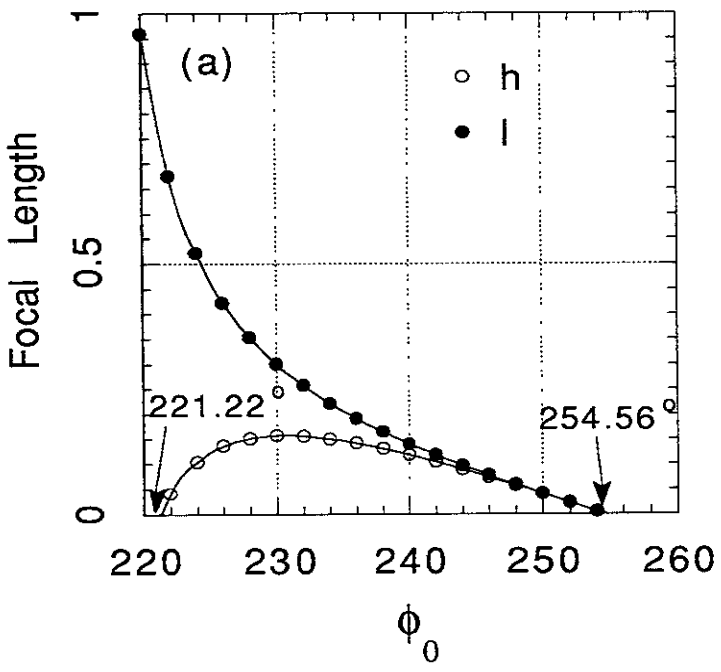

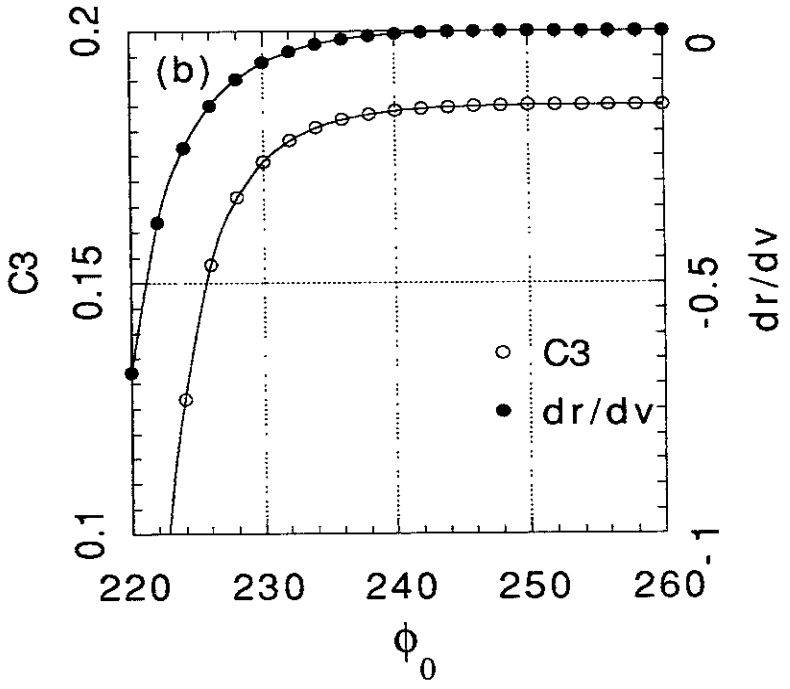

Fig. 3 A. Fujisawa and Y. Hamada

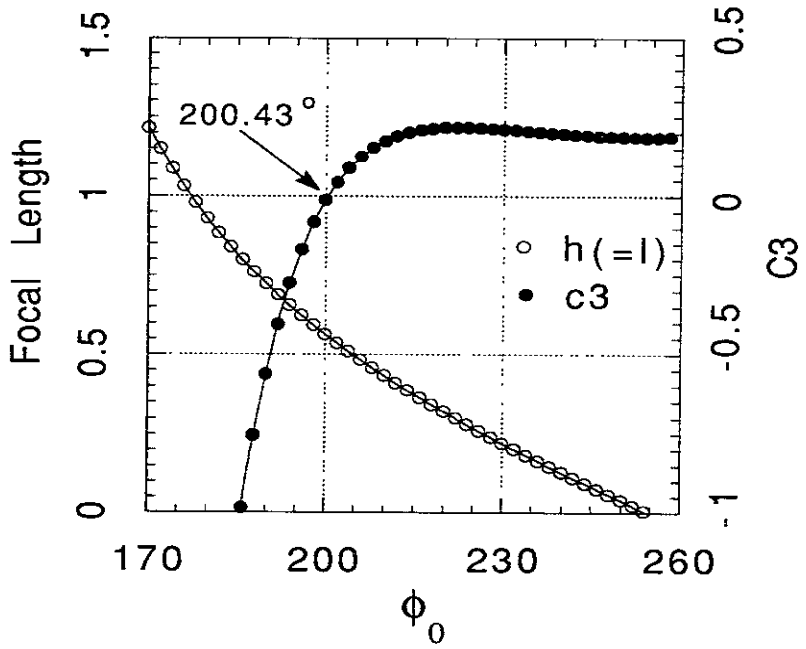

Fig. 4 A. Fujisawa and Y. Hamada

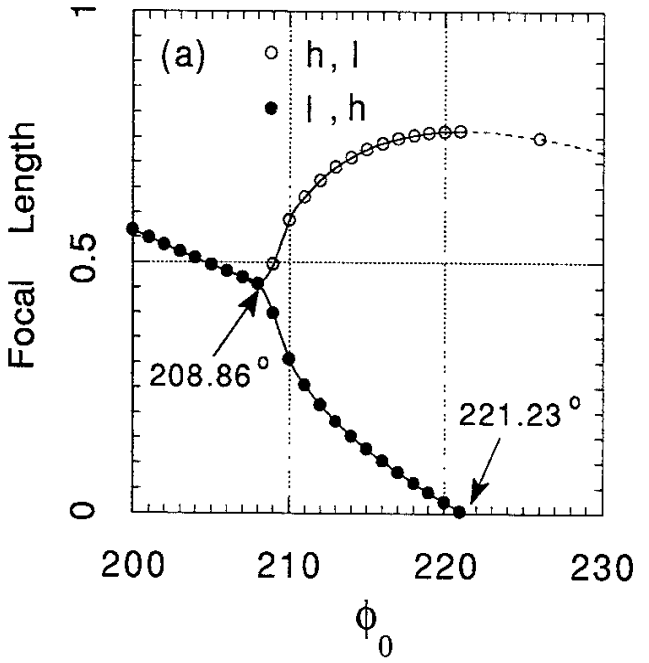

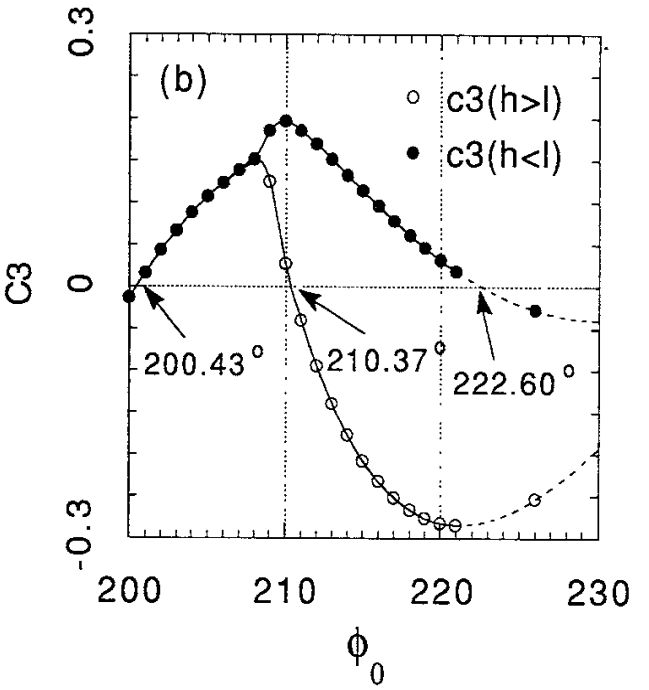

Fig. 5 A. Fujisawa and Y. Hamada

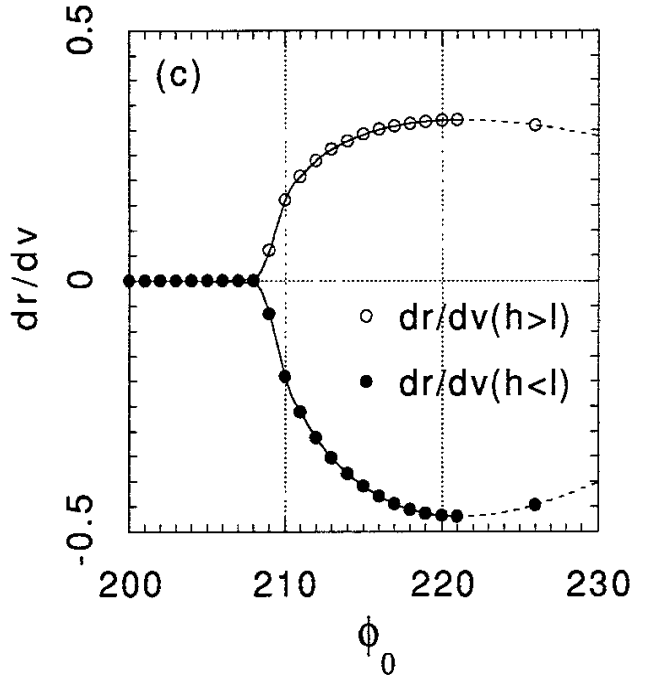

Fig. 5 A. Fujisawa and Y. Hamada

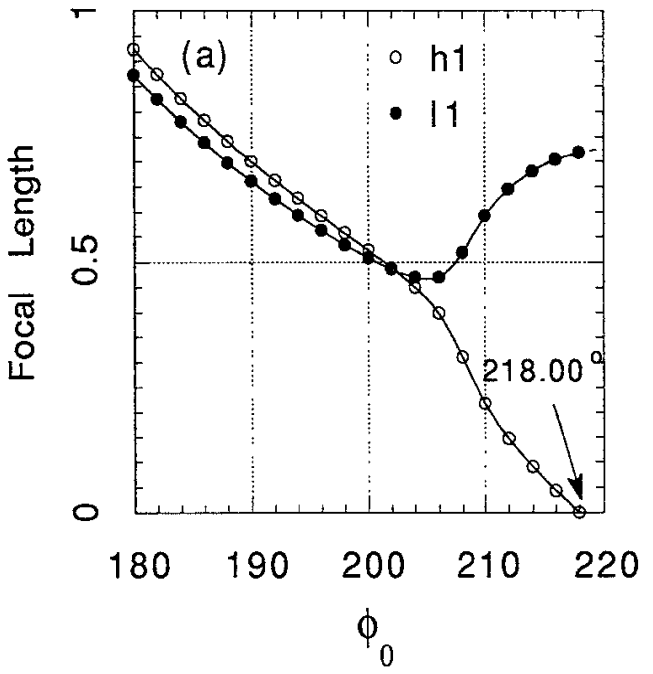

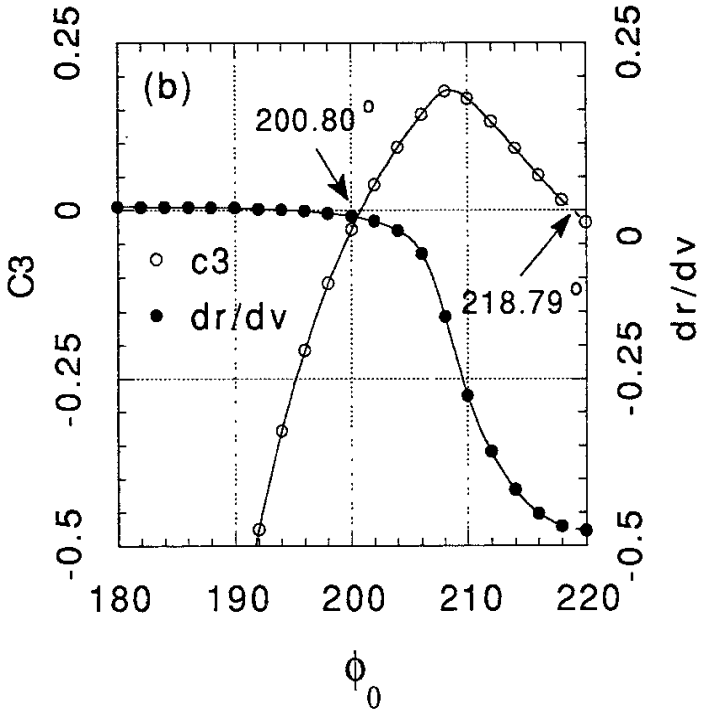

Fig. 6 A. Fujisawa and Y. Hamada

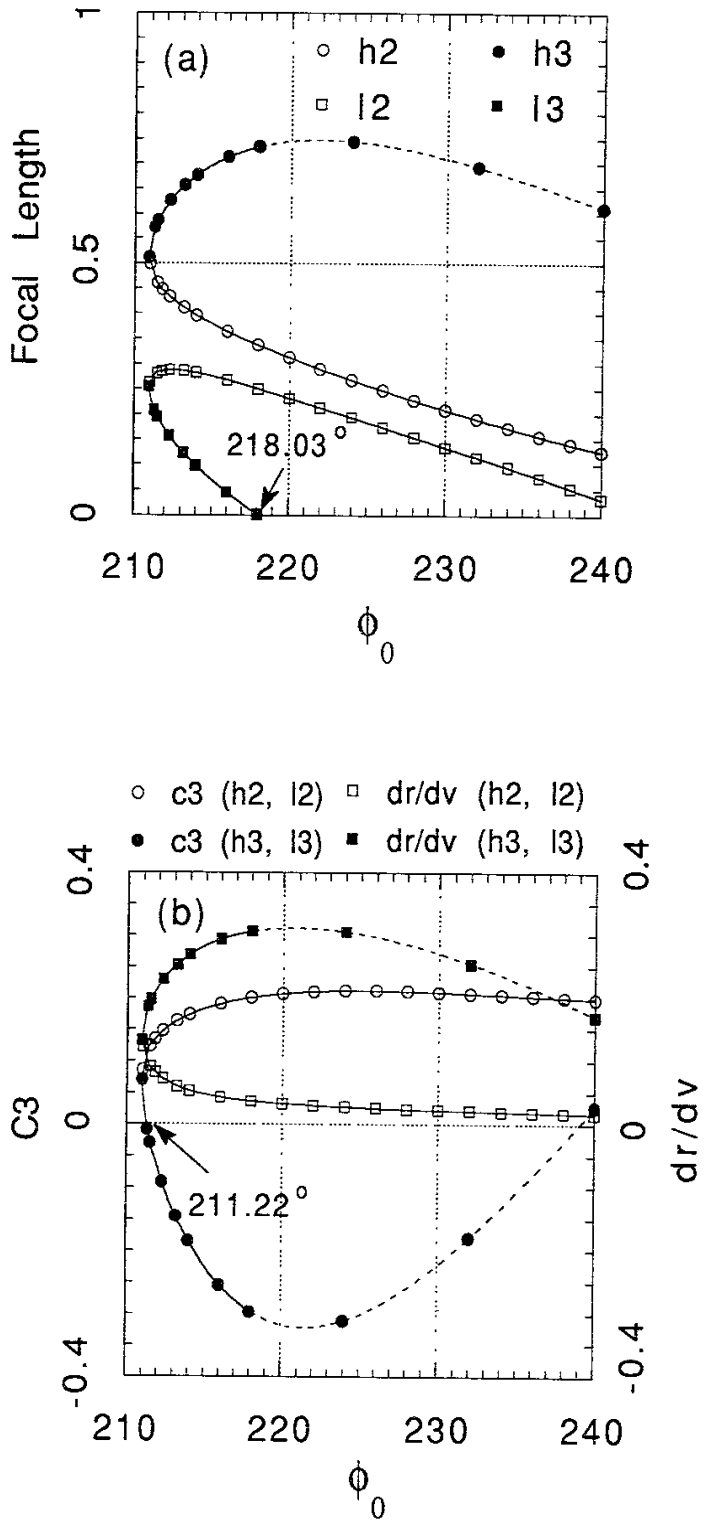

Fig. 7 A. Fujisawa and Y. Hamada

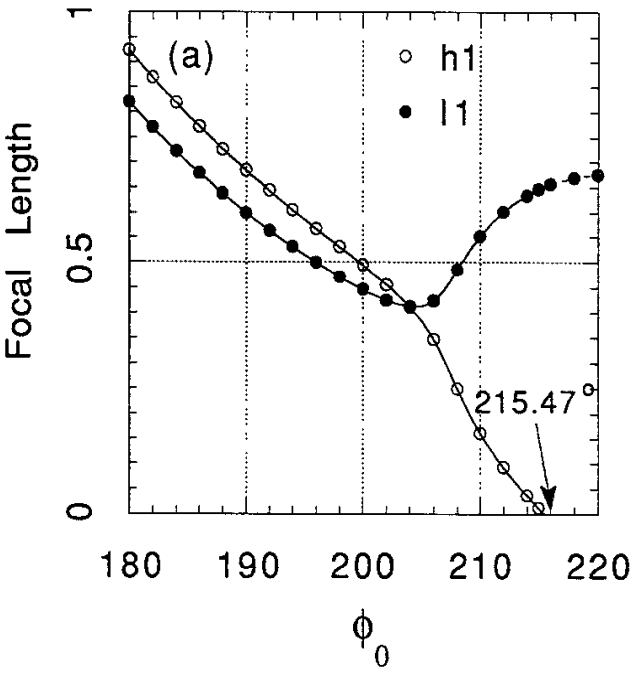

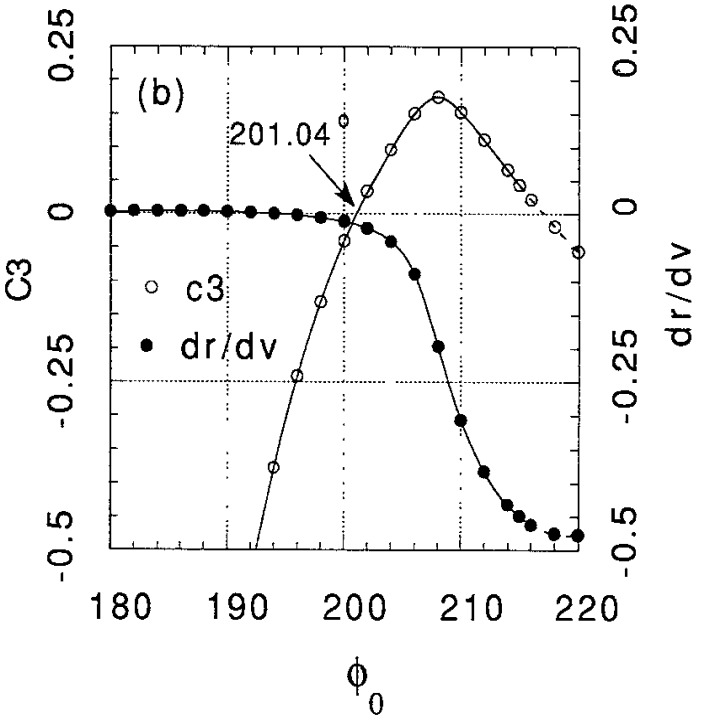

Fig. 8 A. Fujisawa and Y. Hamada

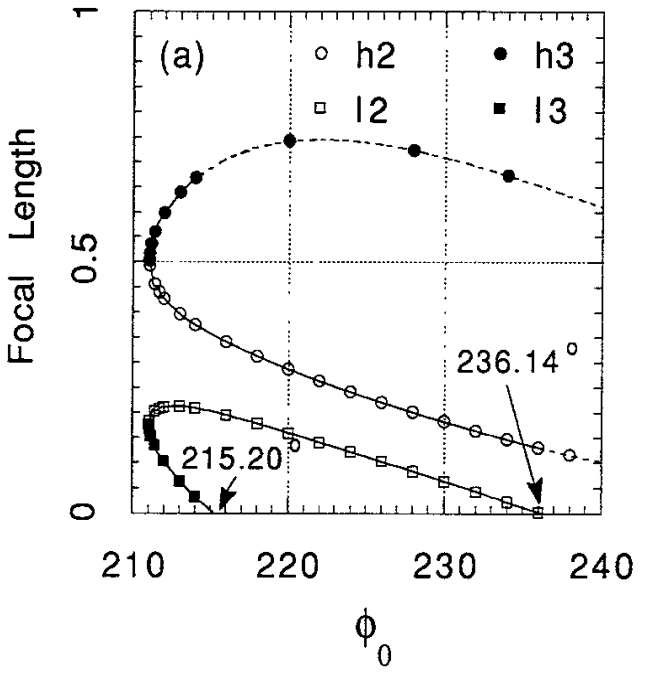

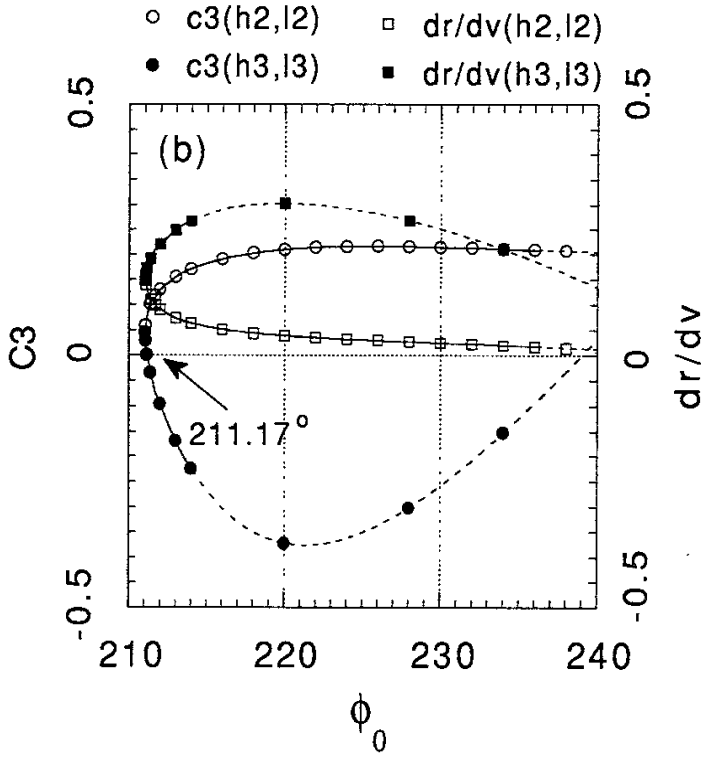

Fig. 9 A. Fujisawa and Y. Hamada

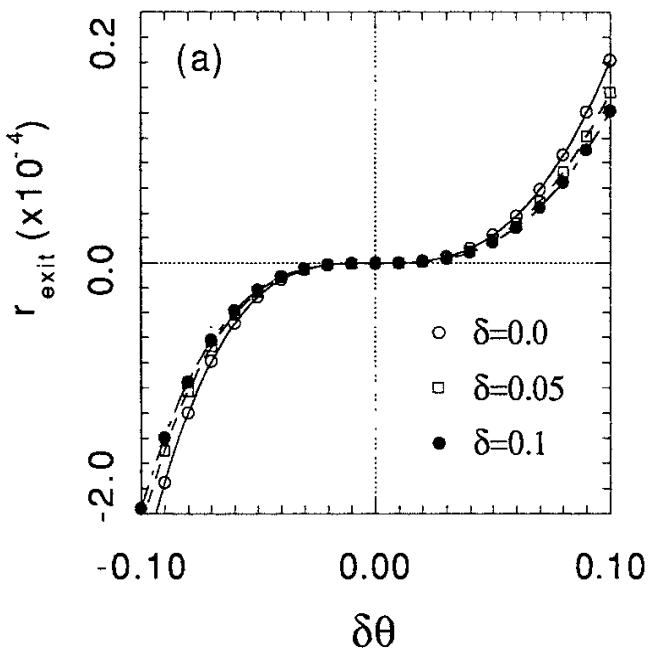

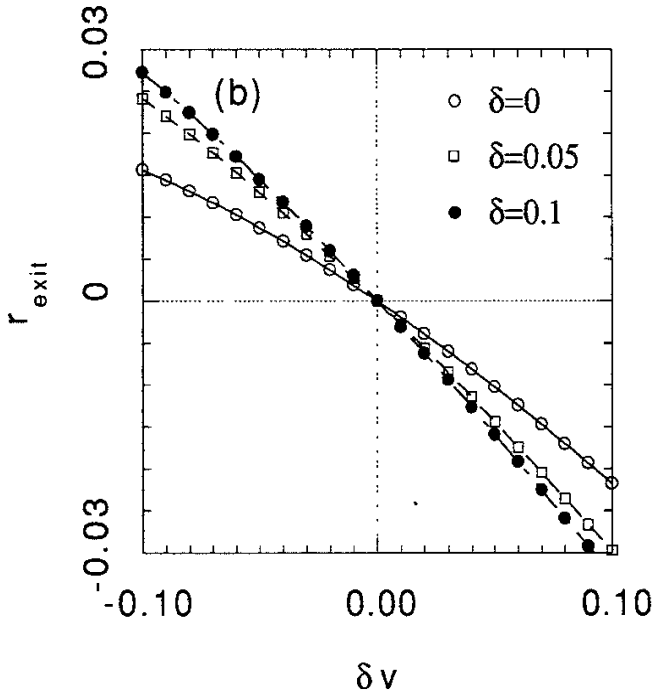

Fig. 10 A. Fujisawa and Y. Hamada

Recent Issues of NIFS Series

NIFS-186 S. Morita, H. Yamada, H. Iguchi, K. Adati, R. Akiyama, H. Arimoto, M. Fujiwara, Y. Hamada, K. Ida, H. Idei, O. Kaneko, K. Kawahata, T. Kawamoto, S. Kubo, R. Kumazawa, K. Matsuoka, T. Morisaki, K. Nishimura, S. Okamura, T. Ozaki, T. Seki, M. Sakurai, S, Sakakibara, A. Sagara, C. Takahashi, Y. Takeiri, H. Takenaga, Y. Takita, K. Toi, K. Tsumori, K. Uchino, M. Ueda, T. Watari, I. Yamada, *A Role of Neutral Hydrogen in CHS Plasmas with Reheat and Collapse and Comparison with JIPP T-IIU Tokamak Plasmas* ; Sep. 1992

NIFS-187 K. Ioth, S.-I. Itoh, A. Fukuyama, M. Yagi and M. Azumi, *Model of the L-Mode Confinement in Tokamaks* ; Sep. 1992

NIFS-188 K. Itoh, A. Fukuyama and S.-I. Itoh, *Beta-Limiting Phenomena in High-Aspect-Ratio Toroidal Helical Plasmas*; Oct. 1992

NIFS-189 K. Itoh, S. -I. Itoh and A. Fukuyama, *Cross Field Ion Motion at Sawtooth Crash* ; Oct. 1992

NIFS-190 N. Noda, Y. Kubota, A. Sagara, N. Ohyabu, K. Akaishi, H. Ji, O. Motojima, M. Hashiba, I. Fujita, T. Hino, T. Yamashina, T. Matsuda, T. Sogabe, T. Matsumoto, K. Kuroda, S. Yamazaki, H. Ise, J. Adachi and T. Suzuki, *Design Study on Divertor Plates of Large Helical Device (LHD)* ; Oct. 1992

NIFS-191 Y. Kondoh, Y. Hosaka and K. Ishii, *Kernel Optimum Nearly-Analytical Discretization (KOND) Algorithm Applied to Parabolic and Hyperbolic Equations* : Oct. 1992

NIFS-192 K. Itoh, M. Yagi, S.-I. Itoh, A. Fukuyama and M. Azumi, *L-Mode Confinement Model Based on Transport-MHD Theory in Tokamaks* ; Oct. 1992

NIFS-193 T. Watari, *Review of Japanese Results on Heating and Current Drive* ; Oct. 1992

NIFS-194 Y. Kondoh, *Eigenfunction for Dissipative Dynamics Operator and Attractor of Dissipative Structure* ; Oct. 1992

NIFS-195 T. Watanabe, H. Oya, K. Watanabe and T. Sato, *Comprehensive Simulation Study on Local and Global Development of Auroral Arcs and Field-Aligned Potentials* ; Oct. 1992

NIFS-196 T. Mori, K. Akaishi, Y. Kubota, O. Motojima, M. Mushiaki, Y. Funato and Y. Hanaoka, *Pumping Experiment of Water on B and LaB_6 Films*

with Electron Beam Evaporator ; Oct., 1992

NIFS-197 T. Kato and K. Masai, *X-ray Spectra from Hinotori Satellite and Suprathermal Electrons* ; Oct. 1992

NIFS-198 K. Toi, S. Okamura, H. Iguchi, H. Yamada, S. Morita, S. Sakakibara, K. Ida, K. Nishimura, K. Matsuoka, R. Akiyama, H. Arimoto, M. Fujiwara, M. Hosokawa, H. Idei, O. Kaneko, S. Kubo, A. Sagara, C. Takahashi, Y. Takeiri, Y. Takita, K. Tsumori, I. Yamada and H. Zushi, *Formation of H-mode Like Transport Barrier in the CHS Heliotron / Torsatron* ; Oct. 1992

NIFS-199 M. Tanaka, *A Kinetic Simulation of Low-Frequency Electromagnetic Phenomena in Inhomogeneous Plasmas of Three-Dimensions* ; Nov. 1992

NIFS-200 K. Itoh, S.-I. Itoh, H. Sanuki and A. Fukuyama, *Roles of Electric Field on Toroidal Magnetic Confinement*, Nov. 1992

NIFS-201 G. Gnudi and T. Hatori, *Hamiltonian for the Toroidal Helical Magnetic Field Lines in the Vacuum*; Nov. 1992

NIFS-202 K. Itoh, S.-I. Itoh and A. Fukuyama, *Physics of Transport Phenomena in Magnetic Confinement Plasmas*; Dec. 1992

NIFS-203 Y. Hamada, Y. Kawasumi, H. Iguchi, A. Fujisawa, Y. Abe and M. Takahashi, *Mesh Effect in a Parallel Plate Analyzer*; Dec. 1992

NIFS-204 T. Okada and H. Tazawa, *Two-Stream Instability for a Light Ion Beam -Plasma System with External Magnetic Field;* Dec. 1992

NIFS-205 M. Osakabe, S. Itoh, Y. Gotoh, M. Sasao and J. Fujita, *A Compact Neutron Counter Telescope with Thick Radiator (Cotetra) for Fusion Experiment*; Jan. 1993

NIFS-206 T. Yabe and F. Xiao, *Tracking Sharp Interface of Two Fluids by the CIP (Cubic-Interpolated Propagation) Scheme*, Jan. 1993

NIFS-207 A. Kageyama, K. Watanabe and T. Sato, *Simulation Study of MHD Dynamo : Convection in a Rotating Spherical Shell*; Feb. 1993

NIFS-208 M. Okamoto and S. Murakami, *Plasma Heating in Toroidal Systems*; Feb. 1993

NIFS-209 K. Masai, *Density Dependence of Line Intensities and Application to Plasma Diagnostics*; Feb. 1993

NIFS-210 K. Ohkubo, M. Hosokawa, S. Kubo, M. Sato, Y. Takita and T. Kuroda,

R&D of Transmission Lines for ECH System ; Feb. 1993

NIFS-211 A. A. Shishkin, K. Y. Watanabe, K. Yamazaki, O. Motojima, D. L. Grekov, M. S. Smirnova and A. V. Zolotukhin, *Some Features of Particle Orbit Behavior in LHD Configurations*; Mar. 1993

NIFS-212 Y. Kondoh, Y. Hosaka and J.-L. Liang, *Demonstration for Novel Self-organization Theory by Three-Dimensional Magnetohydrodynamic Simulation*; Mar. 1993

NIFS-213 K. Itoh, H. Sanuki and S.-I. Itoh, *Thermal and Electric Oscillation Driven by Orbit Loss in Helical Systems*; Mar. 1993

NIFS-214 T. Yamagishi, *Effect of Continuous Eigenvalue Spectrum on Plasma Transport in Toroidal Systems*; Mar. 1993

NIFS-215 K. Ida, K. Itoh, S.-I.Itoh, Y. Miura, JFT-2M Group and A. Fukuyama, *Thickness of the Layer of Strong Radial Electric Field in JFT-2M H-mode Plasmas*; Apr. 1993

NIFS-216 M. Yagi, K. Itoh, S.-I. Itoh, A. Fukuyama and M. Azumi, *Analysis of Current Diffusive Ballooning Mode*; Apr. 1993

NIFS-217 J. Guasp, K. Yamazaki and O. Motojima, *Particle Orbit Analysis for LHD Helical Axis Configurations* ; Apr. 1993

NIFS-218 T. Yabe, T. Ito and M. Okazaki, *Holography Machine HORN-1 for Computer-aided Retrieve of Virtual Three-dimensional Image* ; Apr. 1993

NIFS-219 K. Itoh, S.-I. Itoh, A. Fukuyama, M. Yagi and M. Azumi, *Self-sustained Turbulence and L-Mode Confinement in Toroidal Plasmas* ; Apr. 1993

NIFS-220 T. Watari, R. Kumazawa, T. Mutoh, T. Seki, K. Nishimura and F. Shimpo, *Applications of Non-resonant RF Forces to Improvement of Tokamak Reactor Performances Part I: Application of Ponderomotive Force* ; May 1993

NIFS-221 S.-I. Itoh, K. Itoh, and A. Fukuyama, *ELMy-H mode as Limit Cycle and Transient Responses of H-modes in Tokamaks* ; May 1993

NIFS-222 H. Hojo, M. Inutake, M. Ichimura, R. Katsumata and T. Watanabe, *Interchange Stability Criteria for Anisotropic Central-Cell Plasmas in the Tandem Mirror GAMMA 10 ;* May 1993

NIFS-223 K. Itoh, S.-I. Itoh, M. Yagi, A. Fukuyama and M. Azumi, *Theory of Pseudo-Classical Confinement and Transmutation to L-Mode;* May

1993

NIFS-224 M. Tanaka, *HIDENEK: An Implicit Particle Simulation of Kinetic-MHD Phenomena in Three-Dimensional Plasmas;* May 1993

NIFS-225 H. Hojo and T. Hatori, *Bounce Resonance Heating and Transport in a Magnetic Mirror;* May 1993

NIFS-226 S.-I. Iton, K. Itoh, A. Fukuyama, M. Yagi, *Theory of Anomalous Transport in H-Mode Plasmas;* May 1993

NIFS-227 T. Yamagishi, *Anomalous Cross Field Flux in CHS ;* May 1993

NIFS-228 Y. Ohkouchi, S. Sasaki, S. Takamura, T. Kato, *Effective Emission and Ionization Rate Coefficients of Atomic Carbons in Plasmas;* June 1993

NIFS-229 K. Itoh, M. Yagi, A. Fukuyama, S.-I. Itoh and M. Azumi, *Comment on 'A Mean Field Ohm's Law for Collisionless Plasmas;* June 1993

NIFS-230 H. Idei, K. Ida, H. Sanuki, H. Yamada, H. Iguchi, S. Kubo, R. Akiyama, H. Arimoto, M. Fujiwara, M. Hosokawa, K. Matsuoka, S. Morita, K. Nishimura, K. Ohkubo, S. Okamura, S. Sakakibara, C. Takahashi, Y. Takita, K. Tsumori and I. Yamada, *Transition of Radial Electric Field by Electron Cyclotron Heating in Stellarator Plasmas;* June 1993

NIFS-231 H.J. Gardner and K. Ichiguchi, *Free-Boundary Equilibrium Studies for the Large Helical Device,* June 1993

NIFS-232 K. Itoh, S.-I. Itoh, A. Fukuyama, H. Sanuki and M. Yagi, *Confinement Improvement in H-Mode-Like Plasmas in Helical Systems,* June 1993

NIFS-233 R. Horiuchi and T. Sato, *Collisionless Driven Magnetic Reconnection,* June 1993

NIFS-234 K. Itoh, S.-I. Itoh, A. Fukuyama, M. Yagi and M. *Azumi, Prandtl Number of Toroidal Plasmas;* June 1993

NIFS-235 S. Kawata, S. Kato and S. Kiyokawa , *Screening Constants for Plasma;* June 1993